Supplementary Information

Evaluating magnetic and thermal effects of various Polymerylated magnetic iron oxide nanoparticles for combined chemo-hyperthermia

Kheireddine El-Boubbou,[ab]* O. Mohamed Lemine,[c] Rizwan Ali,[b] Sarah M. Huwaizi,[b] Sulaiman Al-Humaid,[a] and Abdulmohsen AlKushi[a]

[a]Department of Basic Sciences, College of Science & Health Professions (COSHP), King Saud bin Abdulaziz University for Health Sciences (KSAU-HS), King Abdulaziz Medical City, National Guard Health Affairs, Riyadh 11481, Saudi Arabia

[b]King Abdullah International Medical Research Center (KAIMRC), King Abdulaziz Medical City, National Guard Health Affairs, Riyadh 11426, Saudi Arabia

[c]Department of Physics, College of Sciences, Imam Mohammad Ibn Saud Islamic University (IMSIU), Riyadh 11623, Saudi Arabia

To whom correspondence should be addressed: E-mail: elboubboukh@ngha.med.sa; boubbouk@ksau-hs.edu.sa

Contents:

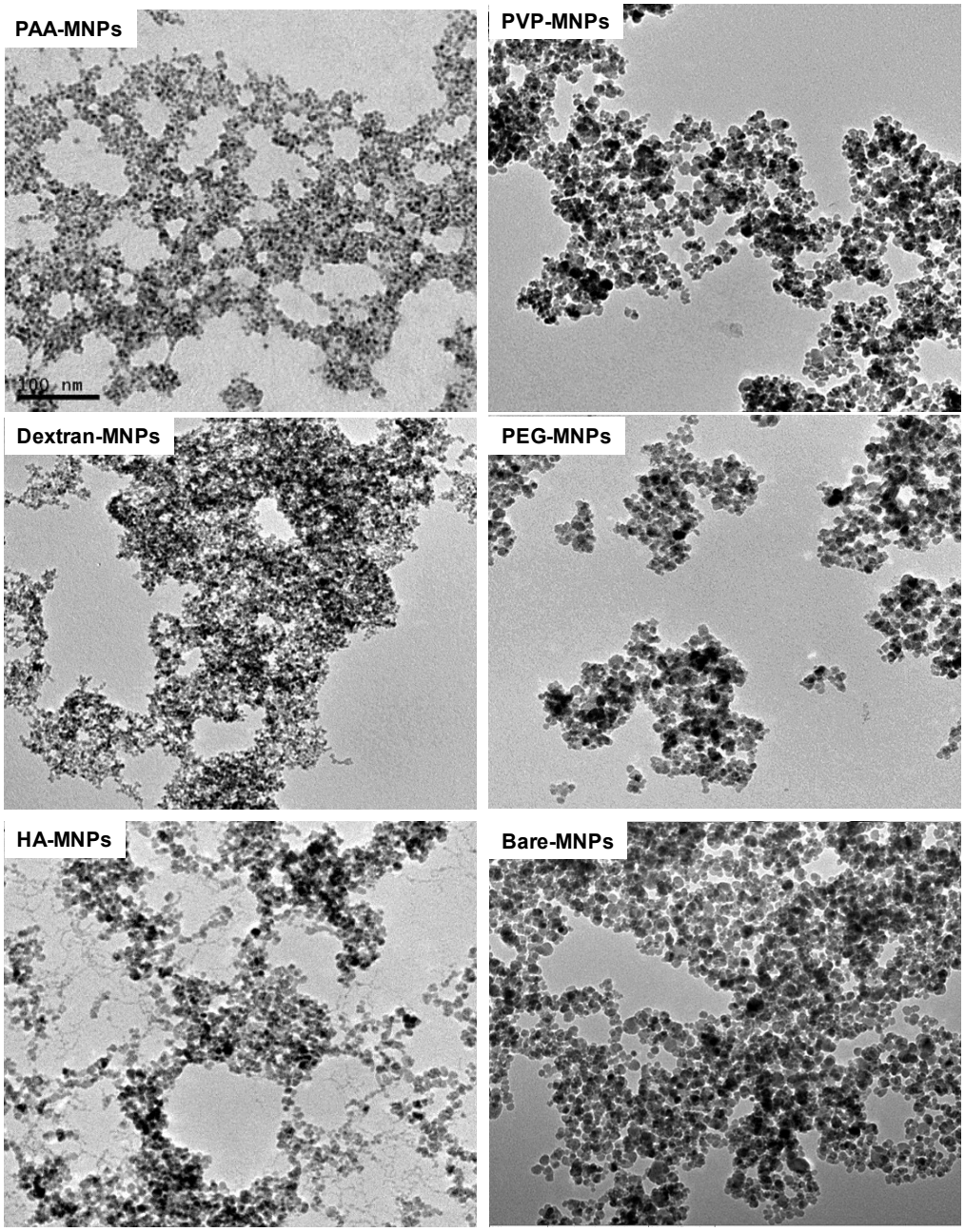

Figure S1. TEM images of the different as-prepared MNPs at 150 k magnification.

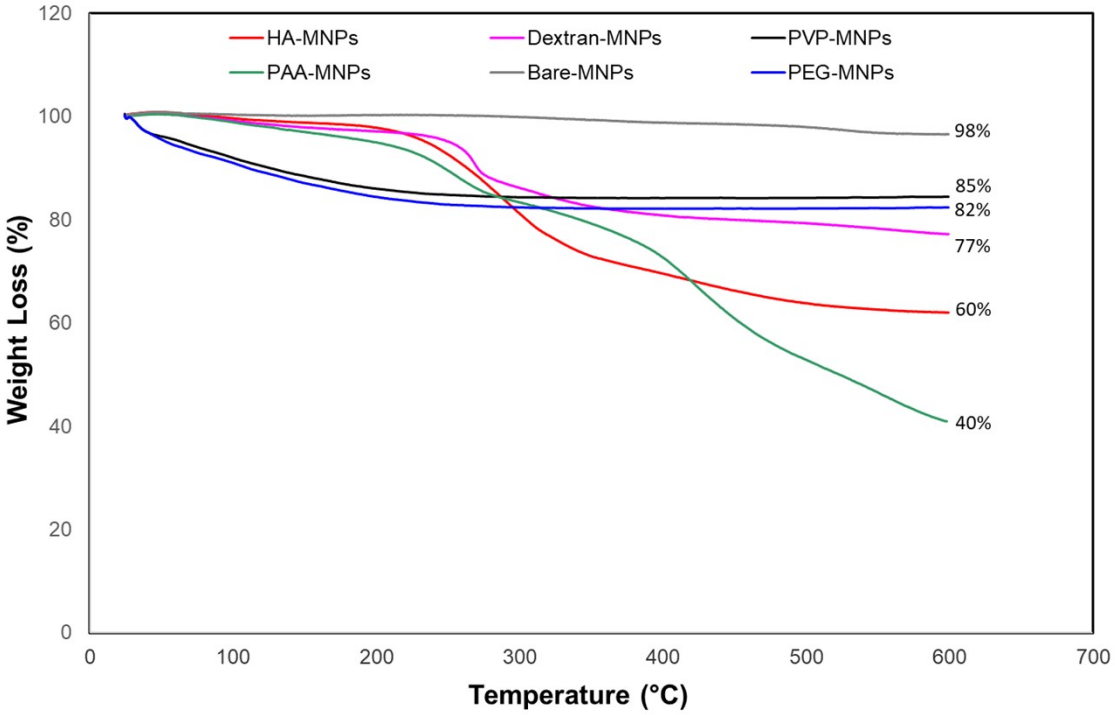

Figure S2. TGA curves for the different MNPs. A total weight loss of 85, 82, 77, 60, and 40% was observed for PVP, PEG, Dextran, HA, and PAA-coated MNPs respectively. It is clearly evident that the grafting of polymers on MNPs was effectively achieved with the lowest surface coating observed for PEG and PVP-MNPs and the highest for PAA-MNPs.

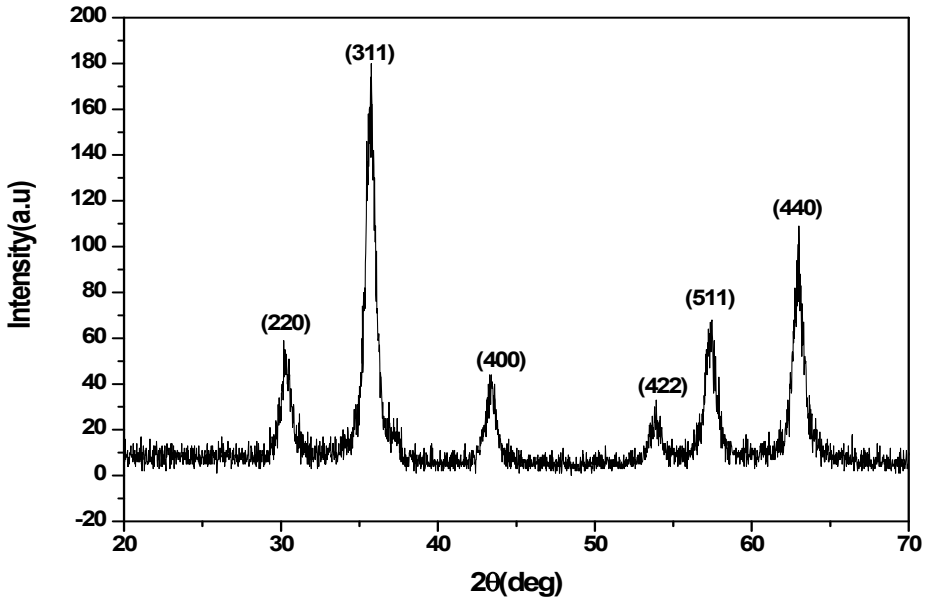

Figure S3. Representative powder XRD of PVP-MNPs with the observed diffraction peaks indicating that the MNPs are magnetite (Fe_3O_4).

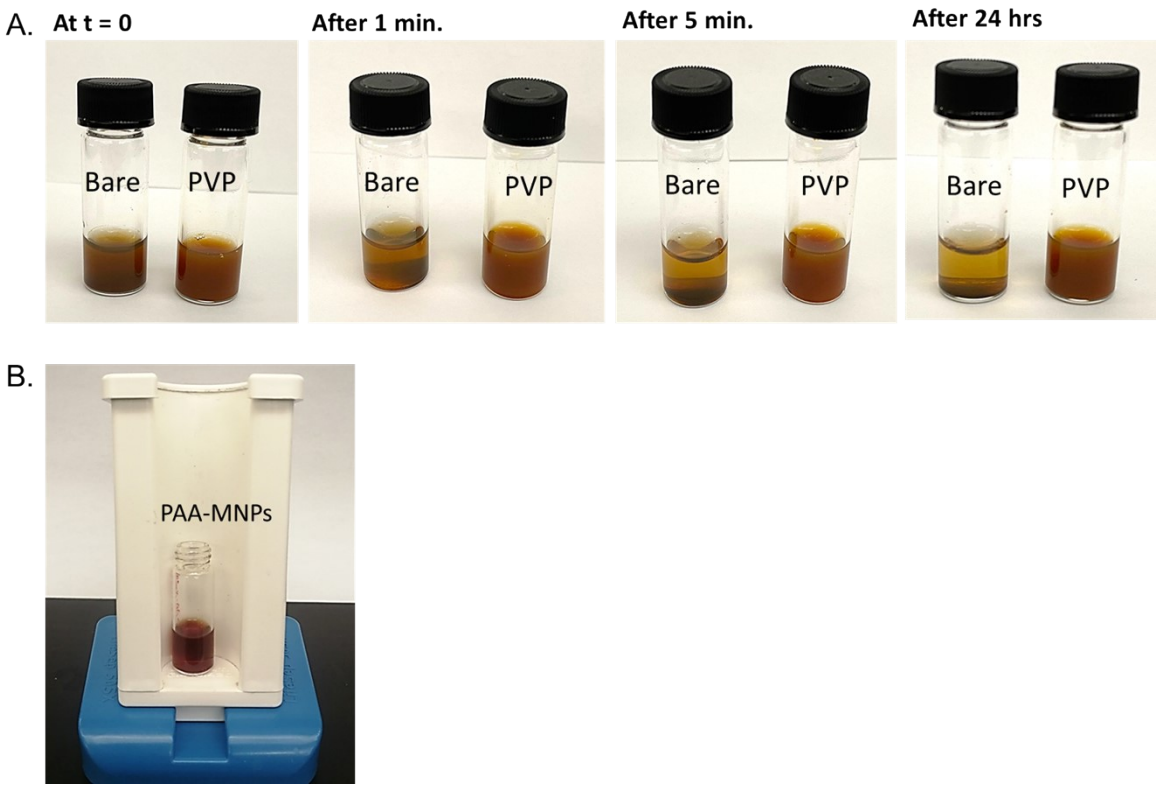

Figure S4. A) Real-time optical photographs of uncoated bare-MNPs and PVP-MNPs clearly showing the fast precipitation of uncoated MNPs and the excellent aqueous dispersity of PVP-MNPs due to the PVP coating. B) Optical photograph of PAA-MNPs showing the ferrofluidic behavior when subjected to external hand-held magnet. No precipitation on the walls of the magnet is observed even after a long time.

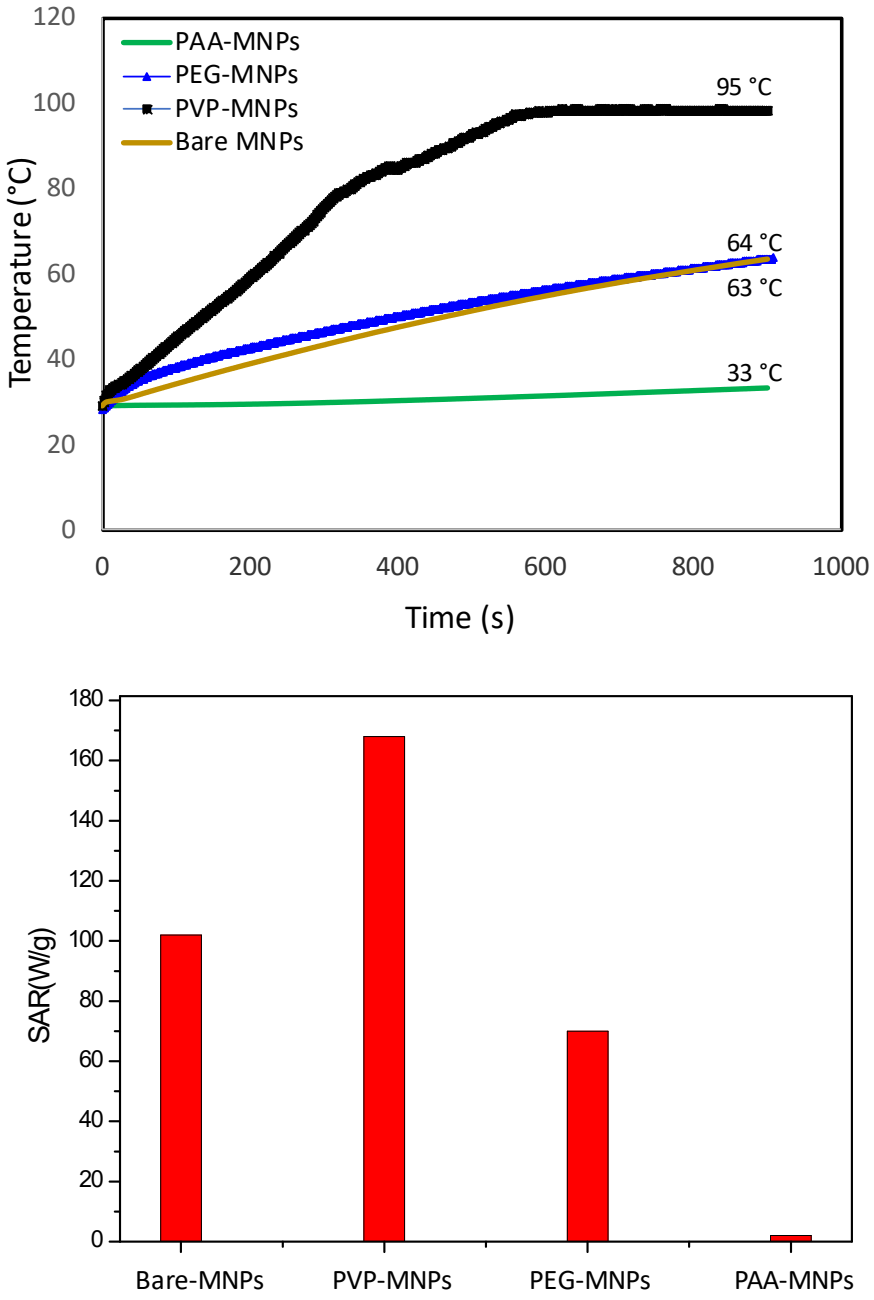

Figure S5. A) Hyperthermia temperature increase *vs* time plots for aqueous dispersions of PMNPs (10 mg/mL) along with their corresponding SAR values (H_0 = 170 Oe and f = 332.8 kHz).

Characterization of Dox@PMNPs:

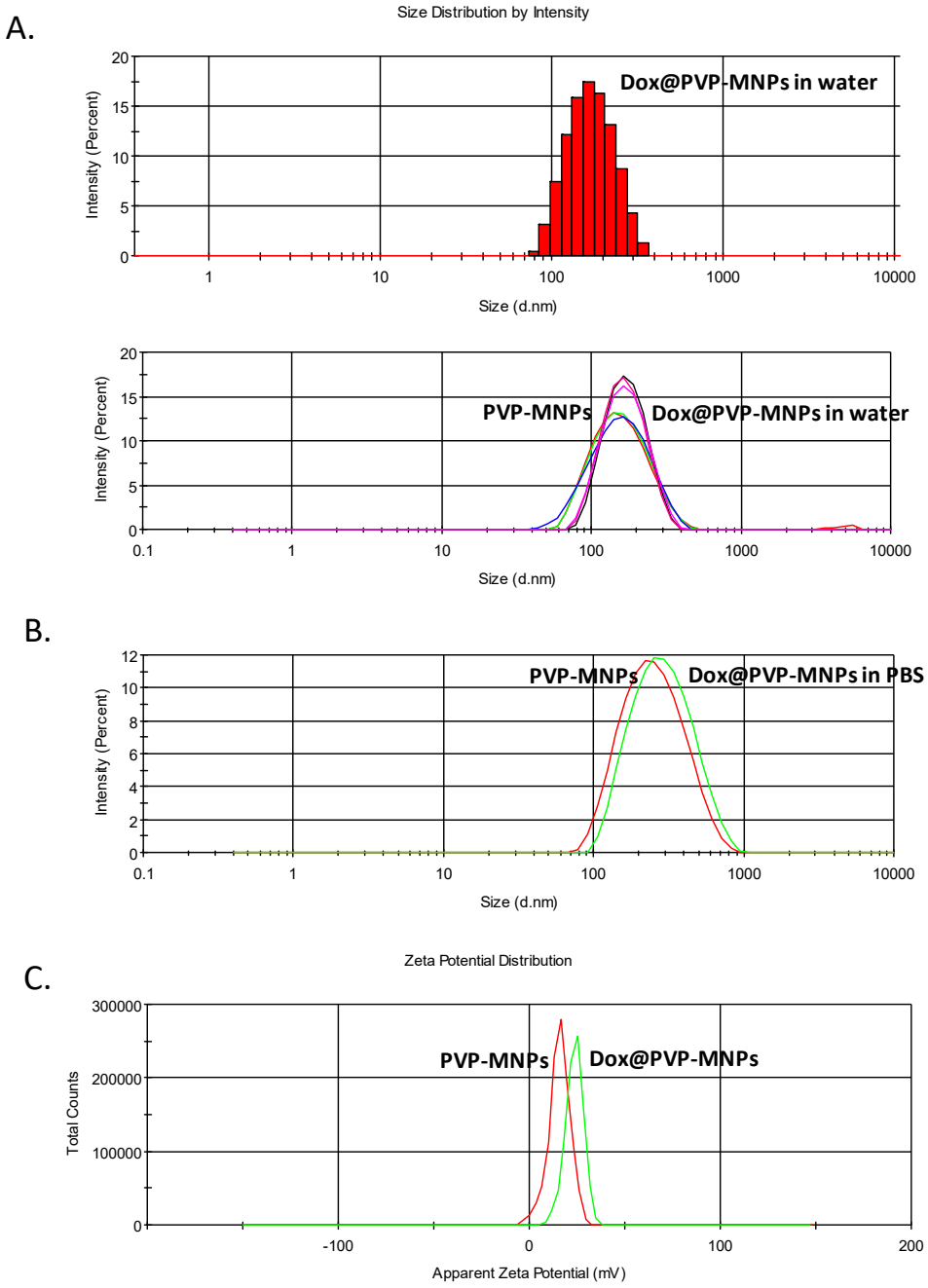

Figure S6. DLS measurements of Dox@PVP-MNPs in water and PBS. A) Hydrodynamic size (D_H) distribution of Dox@PVP-MNPs in water along with a comparison between Dox@PVP-MNPs (D_H = 155 ± 1.31 nm; PDI = 0.09) and PVP-MNPs (D_H = 145 ± 1.99 nm; PDI = 0.15). B) Size distribution of Dox@PVP-MNPs in PBS buffer (D_H = 318 ± 10.90 nm; PDI = 0.323) along with PVP-MNPs in PBS (D_H = 307 ± 11.66 nm; PDI = 0.261). C) Representative zeta potential (ξ) measurements of Dox@PVP-MNPs (ξ = + 15.5 ± 0.99 mV) and PVP-MNPs in water (ξ = + 10.5 ± 1.54 mV). Three independent measurements for three different concentrations were conducted reported as average means ± Std. Dev.

D.

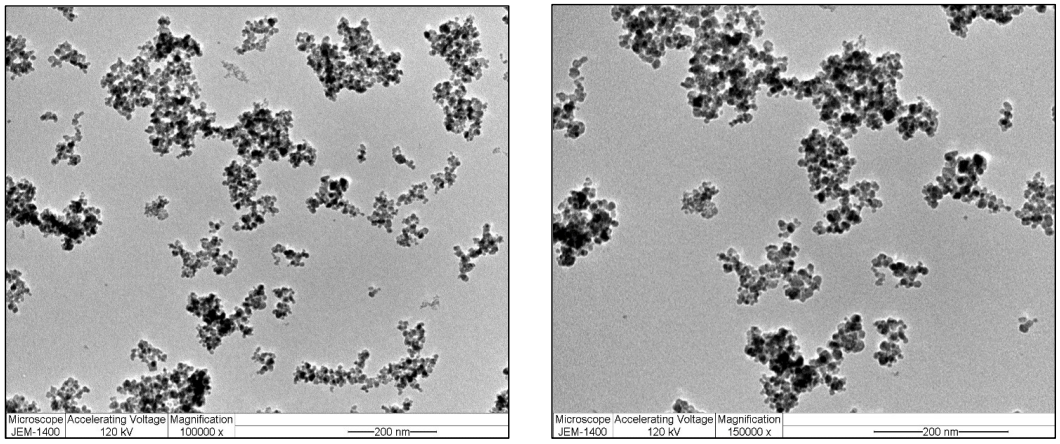

Figure S6. D) TEM images of an aqueous dispersion of Dox@PVP-MNPs at two different magnifications.

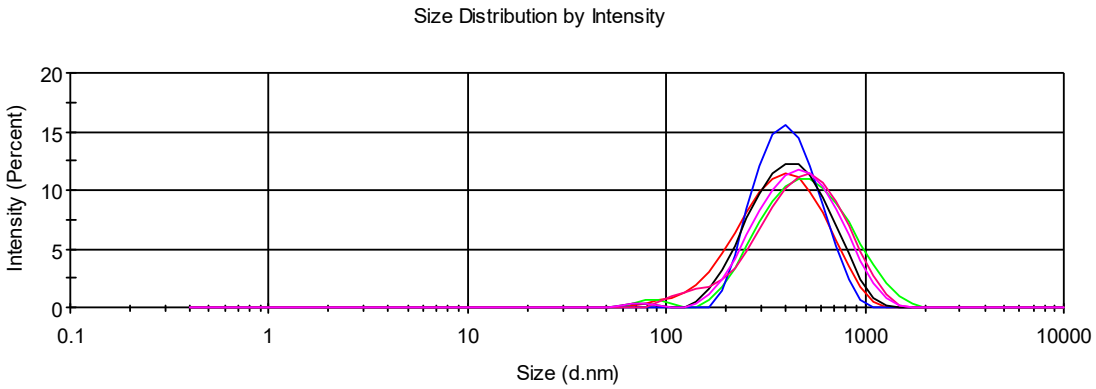

Figure S7. DLS size distribution of PVP-MNPs in PBS buffer monitored over a week.

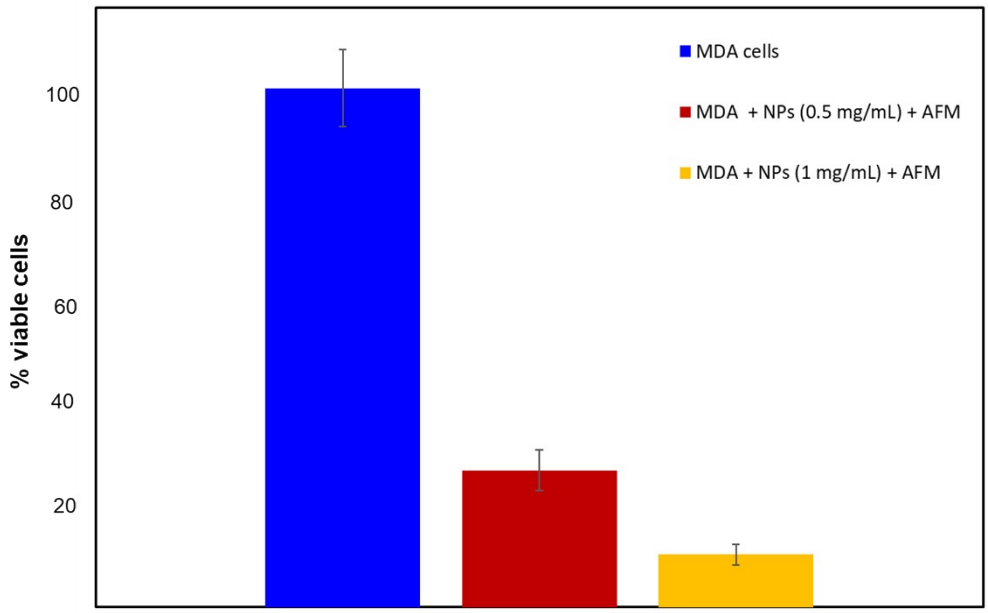

Figure S8. MTT cell viability assay for PVP-MNPs (0.5 mg/mL and 1 mg/mL) treated MDA-MB-231 metastatic breast cancer cells followed by the application of AMF (170 Oe and 332.8 kHz). The experiments were carried out in triplicates and error bars denote standard deviations.

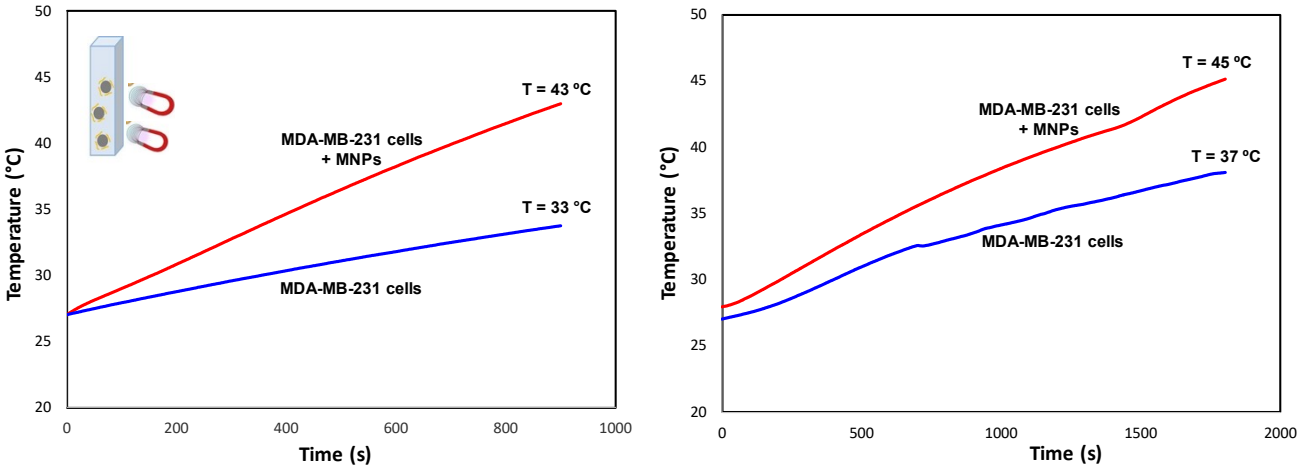

Figure S9. Representative plots of temperature increase *vs* time for PVP-MNPs (**same trend for Dox@PVP-MNPs**) treated with MDA-MB-231 metastatic breast cancer cells followed by the application of AMF (170 Oe and 332.8 kHz) for (left) 15 or (right) 30 minutes.